Aerospace Science and Technology 130 (2022) 107943

Contents lists available at ScienceDirect

Aerospace Science and Technology

www.elsevier.com/locate/aescte

The impact of the ground on flow structure and aerodynamic characteristics of a double delta wing

Mehmet Oguz Tasci [a], Sergen Tumse [a], Besir Sahin [b,*]

[a] Dept. of Mechanical Engineering, Cukurova University, 01330, Saricam, Adana, Turkiye
[b] Dept. of Aerospace Engineering, Istanbul Aydin University, Kucukcekmece, Istanbul, Turkiye

ARTICLE INFO

Article history:
Received 18 April 2022
Received in revised form 23 September 2022
Accepted 7 October 2022
Available online 13 October 2022
Communicated by Gursul Ismet

Keywords:
Aerodynamic coefficients
Double delta wing
Dynamic air cushion
Ground effect
Particle image velocimetry

ABSTRACT

The ground effect (GE) on the formation of the vortical flow over a double delta wing having sweep angles of $\Lambda = 70°/40°$ was examined using the Particle Image Velocimetry (PIV) and dye flow visualization methods in this study. Qualitatively and quantitatively measured results were demonstrated for angles of attack, $\alpha = 15°$ and $25°$ cases in the side and cross-flow planes to reveal the detail of the flow structures. The distance, h between surfaces of the ground and the delta wing normalized with the chord length of the double delta wing, c, was selected as $h/c = 0.1$, 0.25 0.55, and the ground-free case (GFC). The results demonstrated that the magnitudes of the strake and wing vortices at $\alpha = 15°$ and the coiled-up vortex at $\alpha = 25°$ progressively diminish when the delta wing moves from the free-stream region into the boundary layer region close to the ground surface, $h/c = 0.1$. Also, the rate of the inboard movement of leading edge vortices towards the wing central axis increases on the pressure surface of the wing as the altitude of the double delta wing is gradually lowered towards the ground surface. The lift coefficient, C_L of the delta wing enhances due to the development of air stagnation and ram pressure between wing and ground surfaces by lowering the level of the double delta wing from the free-stream region into the boundary layer flow region which is strongly influenced by the presence of the ground surface. Also, the drag coefficient, C_D increases more than the lift coefficient, C_L resulting in a deterioration of the lift to drag ratio, C_L/C_D under the ground effect (GE). Finally, an increment in C_L/C_D is much more prominent at lower angles of attack, α regardless of ground effect.

1. Introduction

Delta wings designed for high speed, have several advantages in terms of structure and aerodynamics. For example, the shock waves occurring at the delta wing-tip with a high sweep angle, Λ, stay below the leading edge of the delta wing, which allows the aircraft to attain high angles of attack, α as indicated by Gursul [1]. Low air friction at high speeds, which is due to the efficiency of the delta wing design, is beneficial for the delta wing to move faster and to have higher lift capacity [2]. However, the maneuvering capacity of these wings is limited due to the formation of the vortex breakdown (VB), which adversely affects the aerodynamic efficiency of the aircraft. It is often aimed at controlling or delaying the development of the VB to improve the maneuverability of the aircraft.

Delery [3] defines the VB as the quick extension of the leading-edge vortex (LEV) structure, the substantial change of the velocity component of the vortical flow, and the formation of significant velocity fluctuations. The VB and the vortical flow formation deteriorate the aerodynamic performance of the delta wing; therefore, it is vital to keep the VB under control. The VB can cause a sudden expansion of the vortical flow structure, severe changes in the velocity field, and the presence of large-scale oscillations, as stated by Payne et al. [7]. Cui et al. [6] discussed the effect of the VB on the aerodynamic behaviors of an aircraft, such that the VB induces a decrease in the lift coefficient, $C_{L,}$ and an increase in the drag coefficient C_D simultaneously. For additional studies about the aerodynamic properties of the wings and the VB, please refer to the previous studies [8–15]. Delta wings are generally categorized as non-slender and slender, depending on the sweep angle, Λ. It is substantially important to classify the delta wings due to a significant variation in their aerodynamic parameters (Canpolat et al. [51]). Munro et al. [4] stated that delta wings are classified as slender when the sweep angle, Λ is larger than or equal to 65°, and delta wings are termed as non-slender if the sweep angle, Λ is lower than 65°. Besides, the double delta wings which can be constructed by the combination of slender and non-slender delta

* Corresponding author.
E-mail address: besirsahin@aydin.edu.tr (B. Sahin).

https://doi.org/10.1016/j.ast.2022.107943
1270-9638/

wings, some other types of configured delta wings are also available (Pevitt and Alam [5]).

Flow structures and aerodynamic characteristics of an aircraft have distinctive features of landing and take-off operations compared to ground-free situation. Despite its importance, the experimental studies on the interactions of the double delta wing and the vortical flow under the influence of the ground surface are limited. Before the main discussion, it is essential to review previous studies about the aircraft runway surface effects on the flow characteristics. It should be noted that the aerodynamic properties of a single delta wing and a double delta are also entirely different. In the present literature, delta wing-runaway surface interactions are generally studied for a single delta wing. Unfortunately, there is no experimental data in the literature, particularly on the double delta wing aerodynamics under the ground effect. However, some numerical efforts about single delta wings moving close to the ground plane are available [16–25].

Lee and Ko [26] experimentally investigated the ground effect on the structure of leading-edge vortices and aerodynamic loadings on a delta wing with a sweeping angle of $\Lambda = 65°$. It is indicated that a significant increase in lift force, F_L, and a relative decrease in drag force, F_D, are observed when the wing moves close to the ground surface during take-offs and landings. As a result, it was found that both the lift force, F_L, and the drag force, F_D, increase with decreasing the ground distance, h/c. According to their study, the ground effect (GE) causes the development of stall to occur earlier and magnifies the formation of leading-edge vortices further with increased rotational speed and expand dimensions of LEVs. Smaller ground clearance results in the stronger leading-edge vortices and earlier vortex breakdown formations.

The GE on the aerodynamic performance of a reverse delta wing which has several anhedrals was investigated by Lee and He [27]. It was concluded that aerodynamic coefficients, C_L and C_D enlarge with the anhedral positioned close to the ground at the wing trailing edge. Nevertheless, when the ground distance, h/c is 0.4 or less, the GE causes a significant increase in C_L. In summary, it is also stated that there is an outboard movement of the LEVs while the delta wing descends towards the ground surface. In the investigation of Wang and Yeung [28], the full and partial ground effects on the lift production of an airfoil that flaps in normal hovering mode were numerically studied utilizing the two-dimensional discrete vortex method. The leading-edge vortex slides down the airfoil's wind side after stroke reversal when the proximity to the ground decreases. The flow separation and the vortical flow formations over a rigid wing and membrane wing under the GE were investigated in the work of Bleischwitz et al. [29]. According to them, membrane wings are observed to deal with adverse pressure gradients which occur with the influence of ground surface, by maintaining the size and structural coherence of tip vortices. Bricteux et al. [30] analyzed the interactions between vortices and turbulent wind as well as the ground throughout the rebound phase that causes the turbulent flow which is fully developed. They revealed that the up-wind vortex exposes vigorous deformations because of the high-scale structures of the wind which hinder the coherent secondary vortex occurrence and causes quicker decay, thus preventing its rebound. The aerodynamic properties of a non-slender delta wing having $\Lambda = 40°$ under the influence of the ground surface were investigated in the experimental studies of Tumse et al. [31]. It is revealed from the results that the lift and drag coefficients (C_L and C_D) gradually increase for all cases of the angle of attack, α, as the wing progressively descends from the ground-free case (GFC) flow region into the flow region affected by the ground surface. Furthermore, the ground distance, h/c, is substantially effective on the aerodynamic behaviors of the wing since the maximum lift-to-drag ratio, C_L/C_D is developed at $h/c = 0.1$. Yin et al. [32] stated that finite obstacles inversely impact the aerodynamic efficiency as the size of the obstacle drops to a critical value. It was revealed that the aerodynamic forces decrease as the wing approaches the obstacle and increase as the wing moves away from the obstacle, contrary to the ground effect.

The vortical flow formation over a double delta wing was explored to ensure the comprehension of the strake/wing vortices and the VB in the previous studies [33]. In addition, the aerodynamics of a cranked double delta wing having rounded and sharp leading edges with sweep angles of $\Lambda = 55°/30°$ were revealed by Manshadi et al. [34]. They reported that the magnitude of the power spectrum density (DPS) reaches the highest value in the vortex core. In the case of the rounded leading edge, primary vortices are formed closer to the wing surface with weaker strength. Karasu and Durhasan [35], and Durhasan and Karasu [36] qualitatively and quantitatively investigated the impact of the kink angle on the aerodynamic attitudes of a double delta wing having a 70° swept slender frontal part in the range of $5° \leq \alpha \leq 35°$ and two Reynolds numbers, $Re = 1 \times 10^4$ and 2.5×10^4 using the dye visualization and the PIV method. It is seen that the interaction between the vortices of the slender frontal part and the posterior part is very high at low angles of attack, and the kink angle, θ is one of the dominant features. The numerical studies on vortical flow structures of a double delta wing with $\Lambda = 80°/65°$ were performed by Liu et al. [37] to demonstrate the instantaneous behavior of VB. It is predicted that locations of VB move forward and backward directions in random motion. The mode of VB transforms due to the variation of VB motion. In addition, the coefficients of the moment C_M, the drag, C_D, and the lift, C_L have a similar trend. The experimental work on the double delta wing having $\Lambda = 70°/50°$ in a wind tunnel using PIV to observe the binary structure of strake vortices was conducted by Zhang et al. [38]. Before the VB, both strake and wing vortices are wrapped around each other. Also, Zhang et al. [39] studied the aerodynamics of a double delta wing having $\Lambda = 70°/50°$ to demonstrate the effect of bleeding and jet blowing. When the jet blowing is applied before the tip of the wing, the strake and wing vortices may be separated. Secondly, employing the jet blowing further downstream is observed to encourage interactions of strake and wing vortices, and hence, these two vortices are combined to form a consistent large vortex.

The current study investigates the vortical flow formation developed over the double delta wing having $\Lambda = 70°/40°$ under the GE with the variation of the ground distance, h/c, as well as the ground-free case (GFC) qualitatively and quantitatively. In this context, the PIV technique and dye visualization method in the water channel and the aerodynamic force measurements in the wind tunnel were carried out. Nevertheless, it is likely to find a few numerical and experimental investigations about the GE on the formation of the vortical flow over the different wing configurations, such as an experimental study of a non-slender delta wing configuration conducted by Tumse et al. [40], a numerical study of a NACA 0012 wing configuration stated by Prasad and Damodaran [41] and an experimental study of a NACA 0015 wing configuration reported by Ahmed and Sharma [42]. However, because of the lack of literature, it is seen that there are not any experimental investigations related to GE on the variation of aerodynamic properties and the formation of the vortical flow field on the double delta wing having $\Lambda = 70°/40°$. The point that distinguishes this study from the other published studies is to investigate the GE on the change of the aerodynamic characteristics of the double delta wing with $\Lambda = 70°/40°$ using qualitative and quantitative techniques. In summary, this study contains groups of dye images, the time-averaged and instantaneous vorticity and streamline patterns, turbulent kinetic energy (TKE), the density of the power spectrum (DPS) analysis of the velocity fluctuations in the vertical direction, and the alteration of the aerodynamic properties of the double

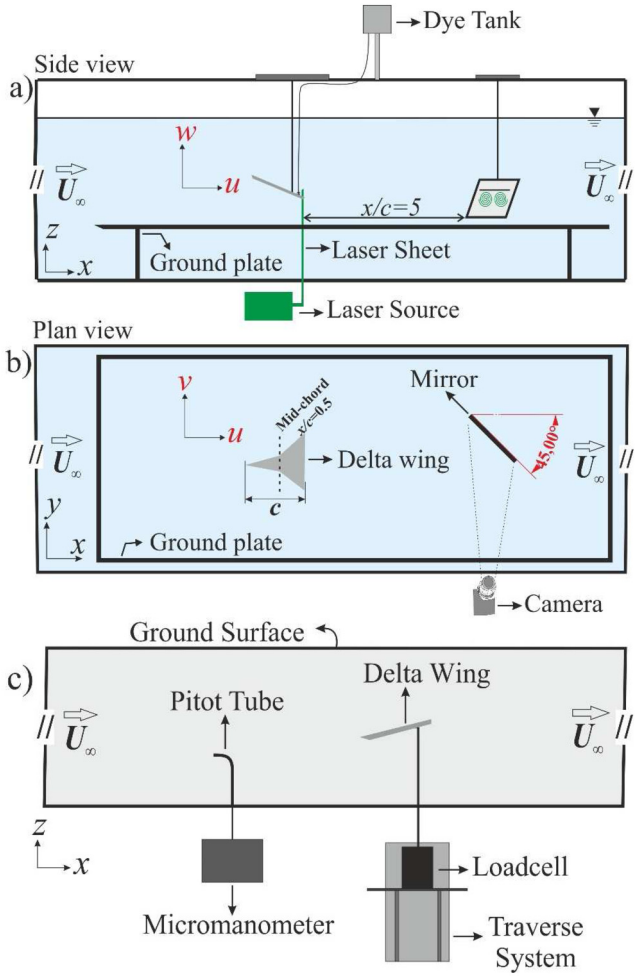

Fig. 1. The demonstration of the experimental arrangements for a) dye flow visualizations in the cross-flow plane b) velocity measurements with the PIV method in the cross-flow plane c) aerodynamic force measurements, F_L and F_D in a wind tunnel.

delta wing disclose the physics of the vortical flow over the double delta wing comprehensively.

2. Material and method

Fig. 1 shows the schematic of experimental setups of the dye observation, the PIV system to measure instantaneous velocity components over the cross-flow and side-view planes, and the 3D force balance system for the measurement of aerodynamic forces in the wind tunnel. As seen in Fig. 1, the PIV technique provides profound information about flow physics to establish a layout for quantitative flow visualization. There are two reservoirs in the water channel positioned at the inlet and the exit of the water channel. The water pump circulates the water between these two tanks. The water passes through the flow regulator with honeycomb geometry which is made up of small cylindrical pipes, before reaching the test section. The water channel depth was 85 cm for conducting experiments. Throughout the experiment, the free-stream velocity was taken as 0.142 m/s. The wing chord length of $C = 180$ mm and a thickness of $t = 5$ mm was used in all quantitative and qualitative experiments. The double delta wing having a strake sweep angle of $\Lambda_s = 70°$ and wing sweep angle of $\Lambda_w = 40°$ was considered in the present work. Also, the leading-edges of the double delta wing made of plexiglass were beveled with 45°. The kink angle was located at the mid-chord of the wing. Since the changes in the vortical flow structure occurring on the delta wing were examined, the delta wing was attached with a cylindrical rod on the suction surface of the delta wing in the vicinity of the trailing edge, so that, it does not affect the VB region and the vortices occurring over the wing surface. The delta wing was attached to the system because of a thin cylindrical rod, which has a negligible effect on the flow structure in the measuring plane. The Reynolds number based on the chord length of the double delta wing was 2.5×10^4 for the whole experiment. The mirror was placed at an angle of 45° to the end-view measuring plane and located about 900 mm ($x/C = 5$) far from the end-view measuring plane downstream of the wing. The ground plate was made of galvanized sheet metal and was long enough to simulate for the free-stream zone and ground effect the flow zone affected by the ground.

The variation of the dimensionless ground distance, h/c was adjusted as 0.1, 0.25, and 0.55 and GFC. The angles of attack of $\alpha = 15°$ and 25° were utilized. The aim for the employment of these angles of attack, α is that the breakdown of the strake and wing vortices is expected to occur over the surface of the double delta wing so that the GE can be seen through the spanwise direction over the double delta wing at the normalized chordwise location of $x/c = 0.8$ for both angles of attack, α.

The PIV system is the velocity measuring device to take the time-dependent velocity distributions over a flow field. Neutrally buoyant silver-coated spherical glass particles with 12 μm-diameters were illuminated by a double-pulsed laser beam at a given period to generate images documented by a CCD camera. This image capturing device receives 15 frames per second with a resolution of 1600×1200 pixels. The spatial resolution of PIV measurements is in millimeter scales, and it is about 1 mm. The average number of particles in the interrogation area was about 35. Bad vectors were eliminated using CLEANVEC software which was written by Meinhart and Soloff [43]. A cross-correlation technique, with 32×32 pixels interrogation windows, was selected to be used with an overlap of 50% to assess the velocity field. Increasing the interrogation window size deteriorates the spatial resolution of PIV analysis. During the experiment, a laser beam was set normal to the flow direction. Uncertainty of the velocity measurements was lower than 2%, as stated by Ozturk et al. [44].

An injector needle attached to a sufficiently long plastic tube coming from the paint tank was inserted into the middle of the delta wing and used to deliver the paint to the tip of the delta wing in a slot buried in the middle axis of the wing. The dye, as it dispersed on the wing surface at a low angle of attack, α sent from the wing tip was sufficient for both the strake and the wing vortex. Since the vortices merge and form a larger united vortex, which is called a "coiled-up vortex", at a high angle of attack, α the dye delivered from the wing tip was sufficient.

High-quality visualization images were obtained by using Rhodamine 6G dye, which changes color between yellow and green tones according to the structure of the vortical flow, under laser light. The SONY HDR-PJ410 camera, accompanied by a special SONY software, was employed to store the view of flow structures and the instantaneous images on electronic devices.

The test zone of the wind tunnel, where the delta wing and measuring elements are positioned, has a square cross-section with dimensions of 570 mm×570 mm and a length of 1000 mm. The Pitot tube was used to control the desired speed. The required forces, F_L and F_D were measured to determine the lift and drag coefficients, C_L and C_D using the formulas as follows:

$$C_L = \frac{F_L}{0.5\rho U_\infty{}^2 A} \tag{1}$$

$$C_D = \frac{F_D}{0.5\rho U_\infty{}^2 A} \tag{2}$$

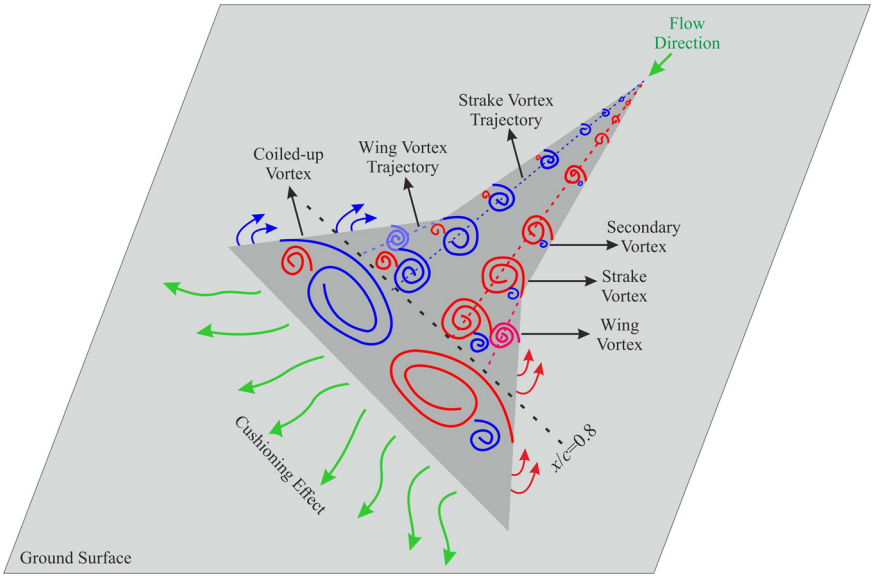

Fig. 2. The schematic illustration of the vortex formation over the double delta wing under the GE.

where ρ (kg/m^3) is the density of water, U_∞ (m/s) is the free-stream velocity, A (m^2) is the planform area of the wing, $A = 0.5 \times b \times c$ in which b and c demonstrate the wing chord length and span of the wing, respectively. The turbulence intensity of the wind tunnel was measured below 0.1%. Uncertainty analysis is essential in examining experimentally obtained results. The uncertainty of the lift coefficient, C_L and drag coefficient, C_D depends on the uncertainties of the load cell, data acquisition card, calibration device, probe position, ambient pressure and air density. Furthermore, the possible measurement errors in adjusting the ground distance, h/c and angle of attack, α were also taken into account. The uncertainty analyses of the lift coefficient, C_L and drag coefficient, C_D were performed considering the methodology reported by Moffat [45]. The results revealed that the uncertainties in the Reynolds number, Re lift coefficient, C_L and drag coefficient, C_D were acquired as 4.6%, 4.9% and 5.1%, respectively. The schematic illustration of the vortex formation over the double delta wing and the VB location has representatively drawn over the double delta wing, and the general properties of the double delta wing and the critical parameters such as Λ, c, s, and h were indicated in Figs. 2 and 3, respectively.

3. Result and discussion

The identification of the strake, the wing, and the secondary vortices over the double delta wing surface at $\alpha = 10°$ in the case of the GFC are qualitatively displayed in Fig. 4. As a flow characteristic of double delta wings, the low and mean angles of attack, α, are more suitable for the definition of vortices. Since high angles of attack, α, cause the flow to stall over the double delta wing, it is not possible to identify the vortices separately, and it is seen that the vortices begin to turn into a large vortex form, which is called "coiled-up vortex". The slender part of double delta wings is sensitive as a function of high angles of attack, α, in the formation of the VB that occurs over the wing. On the other hand, the non-slender part of the double delta wing is even delicate to the low α in the formation of the VB, which reveals the flow physics over the wing in detail. Because of the impact of the sweep angle, Λ on the formations of the vortical flow over the double delta wing, all types of vortices on the double delta wing are visible at a mean α as seen in Fig. 4. The effect of the slender part of the double delta wing causes the formation of the strake vortex. On the other hand, the wing vortex is formed as a result of the non-slender part of

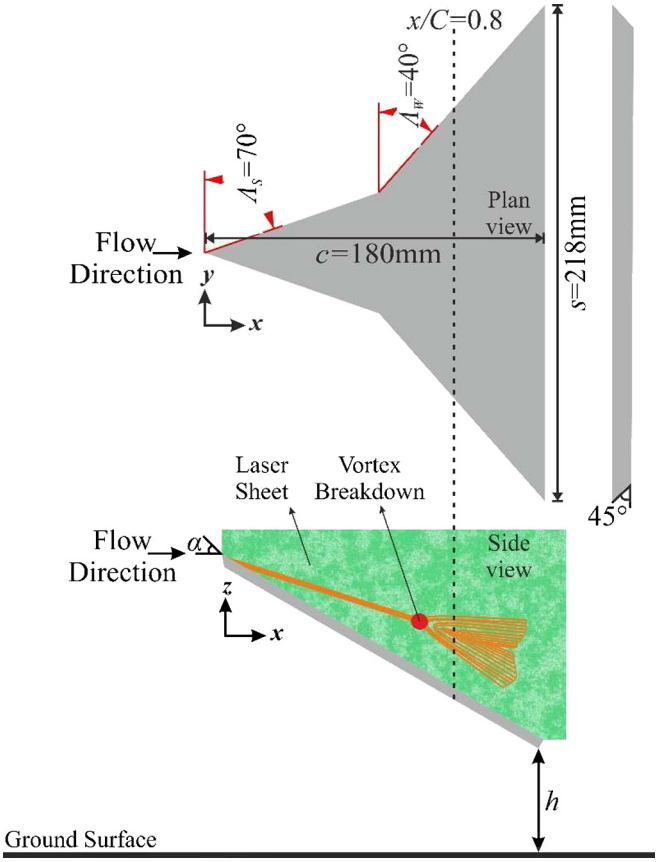

Fig. 3. The definitions of the dimensions of the double delta wing and the critical parameters such as Λ, c, s, and h, and the formation of the vortical flow over the double delta wing.

the double delta wing and the interaction of the flows formed in the slender and non-slender parts of it.

The GE on the alteration of the location of the VB over the double delta wing at $\alpha = 15°$ and 25° under the variations of h/c was qualitatively indicated in Fig. 5. As shown in Fig. 5, it is observed in the plan-view plane that the strake vortex over the double delta wing takes place dominantly in comparison with the wing vor-

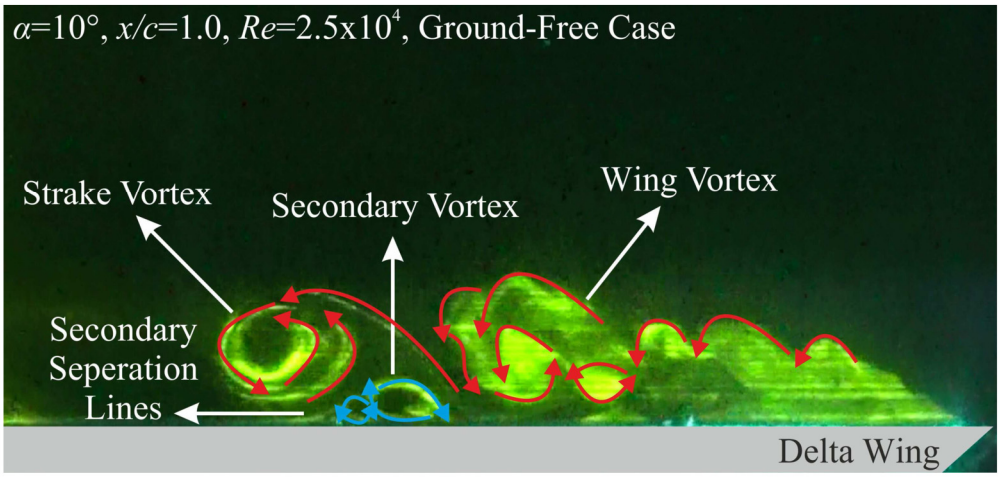

Fig. 4. The identification of the strake, wing, and secondary vortices over the double delta wing at $\alpha = 10°$.

tex and moves towards the center of the double delta wing. The VB position at $\alpha = 15°$ is found to occur at an earlier stage compared to the GFC. For instance, while the VB position for the GFC is found to be $x/c = 1.04$, the onset of VB for $h/c = 0.10$ occurs at a distance of $x/c = 0.78$. Correspondingly, the location of VB of the coiled-up vortex that occurred at an earlier stage is noticed over the wing surface under the GE in comparison with the GFC at $\alpha = 25°$. For example, while the VB locations are detected as $x/c = 0.64$ and 0.68 for $h/c = 0.55$ and GFC, respectively, however, the location of the VB moves towards to the apex of the double delta wing, and it is observed at $x/c = 0.59$ for the $h/c = 0.10$ case. The GE causes the coiled-up vortex to induce an earlier VB because of growth in the gradient of the adverse pressure on the bottom of the double delta wing through the chordwise direction. As seen in Fig. 5, the amplitude of the fluctuations in the VB location increases as the double delta wing moves towards the ground surface because of the disorganized and irregular flow structures. In the GFC, the amplitude of the fluctuations in the VB location is found more stable compared to the case of $h/c = 0.10$.

Fig. 6 demonstrates the influences of the ground surface on the time-averaged streamline, $< \psi >$ patterns at $\alpha = 15°$ under the variations of h/c. Here, definitions of F_s, F_w, z_s/s, z_w/s, y_v/s, and θ_{sw} are identified to describe flow data in this figure. However, z_s/s and z_w/s, are used to define the distance between the foci of the strake, F_s and wing vortices, F_w with the wing surface. On the other hand, y_v/s is the distance between the foci of the strake, F_s and wing vortices, F_w. The distances on the flow characteristics, z_s, z_w, and y_v, are normalized with the semi-span length, s. Finally, θ_{sw} is the rotational angle between the foci of the strake, F_s and wing vortices, F_w as also indicated in the study of Zhang et al. [38]. It turns out that z_s/s decreases significantly when the double delta wing descends from the ground-independent flow region to the ground affected flow region at $h/c = 0.10$. It can be interpreted that as the distance of the wing to the ground decreases, the ground effect causes the intensity of the interaction between the vortical flow and the wing surface to increase. For example, the dimensionless distance z_s/s is detected as 0.181 in the case of excessive ground effect on the flow at $h/c = 0.10$, while the dimensionless distance z_s/s is determined as 0.196 in the absence of ground effect on the flow. Although the interaction between the flow and the wing surface increases because of the GE, the impact of the dynamic air cushion caused by the rise of adverse pressure gradient at the bottom of the double delta wing, through the chordwise direction, the air stagnation in the region between the ground and the double delta wing, causes the wing vortex to move away from the delta wing surface. As can be seen from Fig. 6b, the

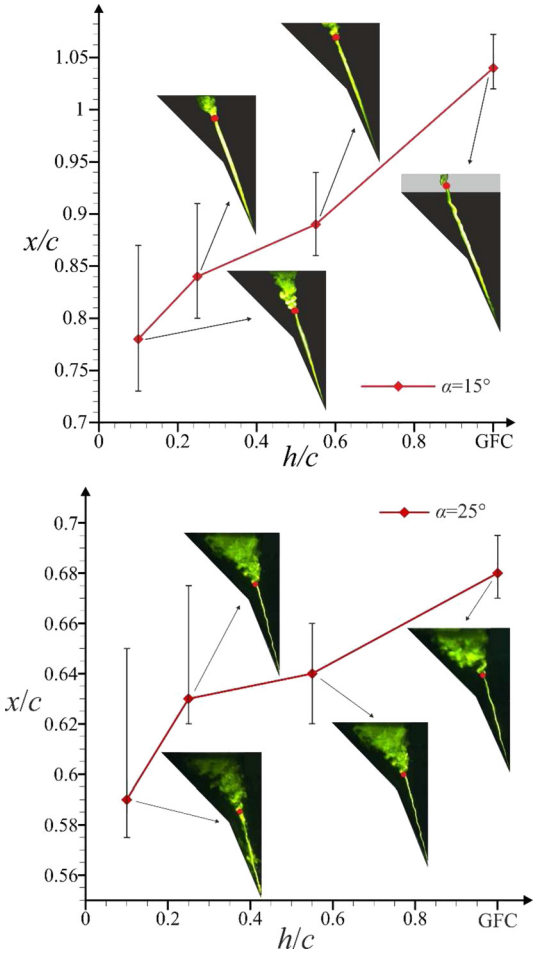

Fig. 5. The formation of the VB over the double delta wing at $\alpha = 15°$ and 25° under the variations of h/c.

height of the wing vortex, z_w/s, increases as the double delta wing gets closer to the ground surface. For example, while z_w/s was observed as 0.139 in the case of GFC, it was observed that z_w/s is equal to 0.153 at $h/c = 0.10$. Because of air cushioning, there is a decrease in the rotational angle, θ_{sw}, between the strake and wing vortices. For example, θ_{sw} was detected as 6.4° in the case of $h/c = 0.10$, while θ_{sw} was 10.4° in the case of GFC. In addition, the distance between the strake vortex and wing vortices, y_v/s, also decreases as a result of earlier VB and the vortices converge

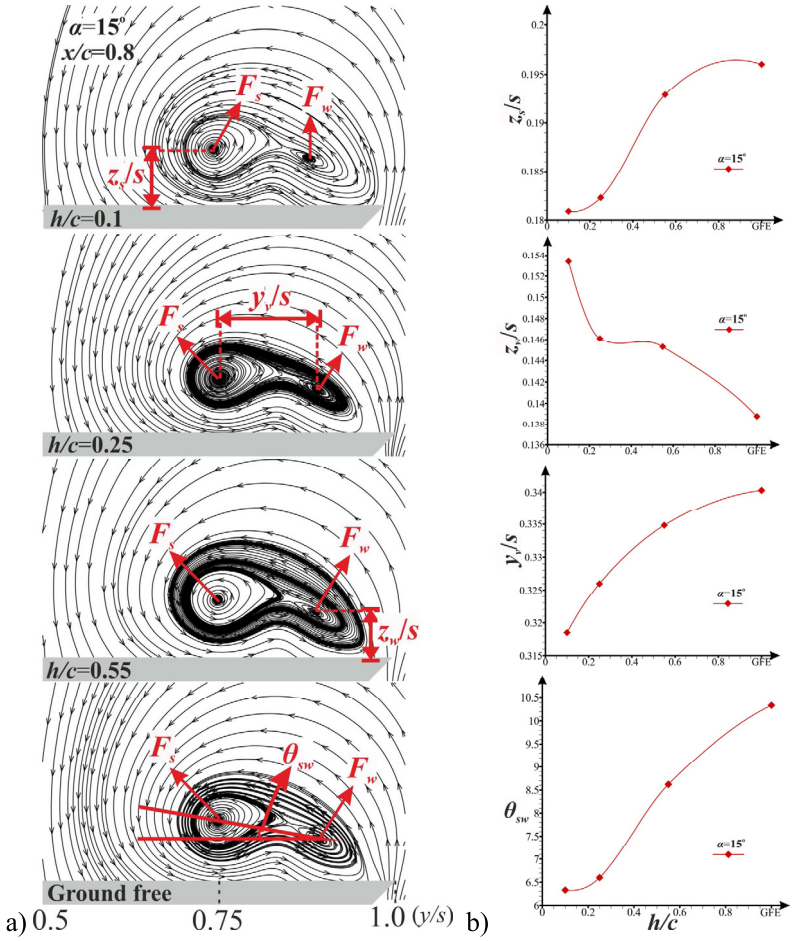

Fig. 6. a) The patterns of the time-averaged streamline, $< \psi >$ in the cross-flow plane at $\alpha = 15°$ under the variations of h/c. b) The alteration of the flow characteristics over the double delta wing is presented by the patterns of the time-averaged streamlines, $< \psi >$ at $\alpha = 15°$.

with each other as revealed in the study by Zhang et al. [38]. For example, while y_v/s is found to be equal to 0.338 in the case of GFC, this value decreases to 0.318 when the position of the double delta wing declines from the region of GFC close to the location of $h/c = 0.10$.

Fig. 7 represents the alteration of the flow characteristics over the double delta wing presented by the patterns of the time-averaged streamlines, $< \psi >$ under the GE at $\alpha = 25°$ with the variations of h/c. Here, F_c is used to describe the focal point of the coiled-up vortex. Also, in Fig. 7, the ground effect as a function of the distance, y_f between the middle of the semi span of the wing and the location of the foci, F is normalized with the semi span length, s and symbolized as y_f/s is presented. It is indicated from Fig. 7b that the inboard movement of the coiled-up vortex along the spanwise direction over the double delta wing occurs under the GE; in other words, the foci of the coiled-up vortex, F_c move toward the central axis of the wing as the location of the double delta wing is lowered to a level $h/c = 0.1$. For example, while the change of the distance between the middle of the semi span and the location of foci is found to be $y_f/s = 0.098$ in the region of GFC, the foci of the coiled-up vortex, F_c moves towards the wing center to locations of $y_f/s = 0.134$ and 0.216 when the double delta wing descends from the GFC region to levels $h/c = 0.55$ and 0.1 cases, respectively.

The patterns of the time-averaged streamlines, $< \psi >$ under the GE with the variations of h/c at $\alpha = 25°$ in side-view planes were demonstrated in Fig. 8. The results were measured only over a specified portion of the flow field throughout the complete chord of the double delta wing to define the exact location of the VB and its size, which is one-third of the chord length. The VB locations can also be viewed in Fig. 5 with the dye observations. The parameter of z/s is a normalized distance, and it is expressed as the distance, z between the wing surface and the VB position divided by the span length, s. As seen from Fig. 8, z/s decreases when the double delta wing descends from the region of GFC into the region affected by the presence of the ground surface, revealing that the rate of interactions between the wing surface and the vortical flow is magnified. For example, while z/s is equal to 0.075 in the region of GFC, then z/s is found to be 0.067 and 0.062 when the position of the double delta wing is lowered from the region of GFC to levels $h/c = 0.55$ and 0.1 cases, respectively. In addition, the interaction between the vortical flow and the wing surface continues to increase in line with the decrease in h/c, resulting in an earlier VB formation and, therefore, irregularities in the vertical flow structures downstream of the VB continue to increase. In other words, the amplified irregularities in the vortical flow result in an increment in the complexity and intensity of unsteady flow, which may cause the wings to vibrate, and hence an attenuation of aerodynamic performance takes place as reported by Gursul [1]. However, it is observed that the vortex symmetry worsens as the double delta wing moves from the flow region where there is no ground surface effect to the flow region where the ground effect is very intense.

The influences of the ground on the structure and the magnitude of the concentration of the strake, wing, and secondary vortices which are seen over the double delta wing at $\alpha = 15°$ and

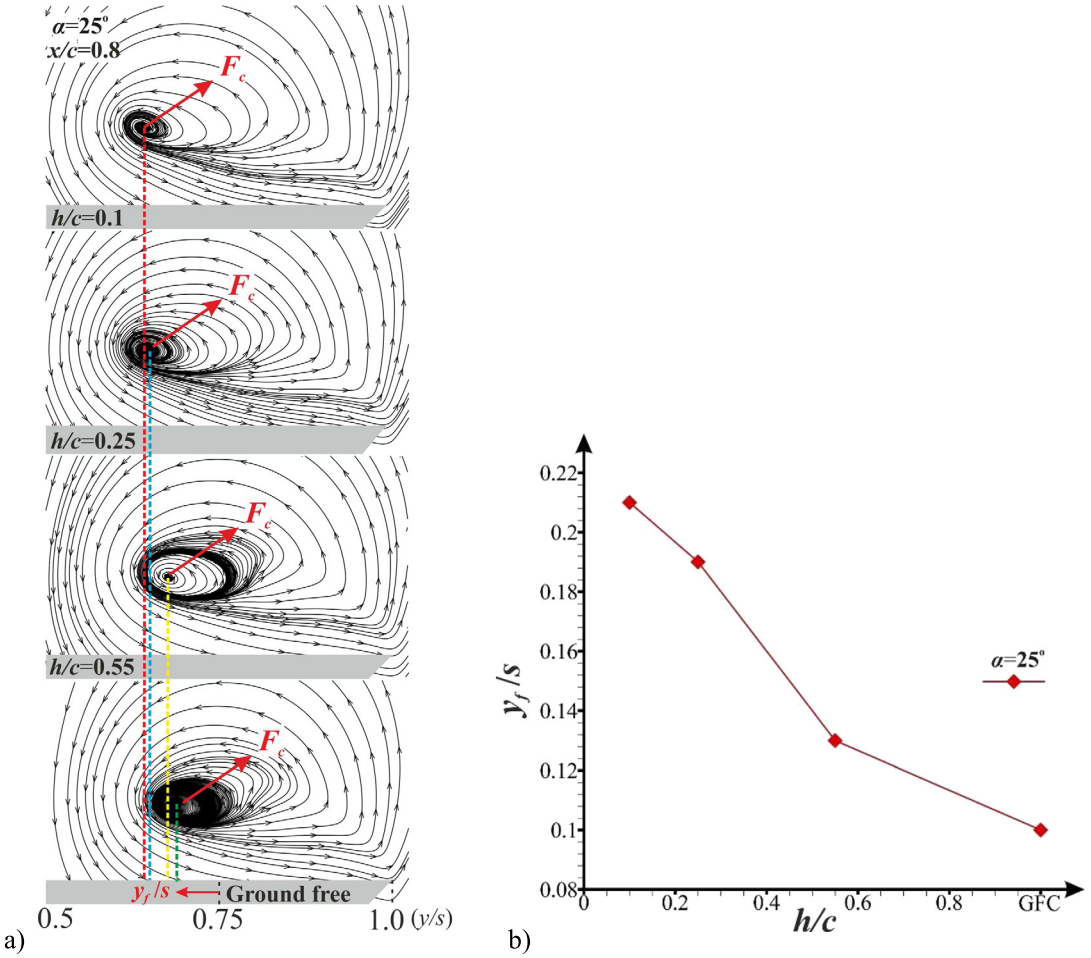

Fig. 7. a) The change of the time-averaged streamline patterns at $\alpha = 25°$ with the variations of h/c. b) The alteration of the distance from the middle of semi-plan to foci points on the patterns of the time-averaged streamline, y_f/s in the cross-flow plane.

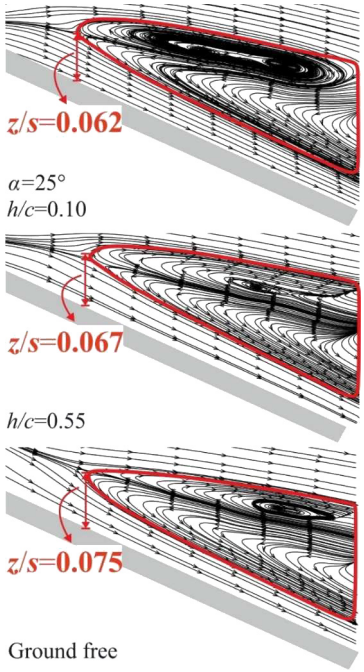

Fig. 8. The alteration of the dimensionless distance, z/s presented by the time-averaged streamline patterns, $< \psi >$ between the surface of the double delta wing and the VB location with the variations of h/c in the side-view plane at $\alpha = 25$.

the coiled-up vortex at $\alpha = 25°$ are indicated in Fig. 9. The secondary vortices rotated in the opposite direction of the strake and wing vortices are formed because of the flow separation induced by the interaction between the strake vortices and the boundary layer of the double delta wing. The magnitude of the vorticity concentration is normalized as $w^* = wc/U_\infty$. Furthermore, the maximum magnitude of the dimensionless vorticity concentration, $w^* = wc/U_\infty$, in the core region of the coiled-up vortex slightly decreases at $\alpha = 25°$ when the double delta wing moves from the ground free effect flow region to the flow region where ground effect exists as seen in Fig. 9. However, the normalized intensity of the strake, wing, and secondary vorticities gradually drops when the double delta wing position is lowered to a level close to the wing surface at $\alpha = 15°$ the GE induces an earlier VB. For example, the normalized intensity of the strake, wing, and secondary vorticities are found to be ${w_{st}}^* = 52$, ${w_w}^* = 24.2$, and ${w_s}^* - 24.1$ at $\alpha = 15°$ at the GFC, respectively. On the other hand, the magnitudes of these vorticities, ${w_{st}}^*$, ${w_w}^*$ and ${w_s}^*$ progressively decrease as ${w_{st}}^* = 51.2$, 49.8, and 49.4 as strake vorticity, and ${w_w}^* = 23.4$, 22.2, and 21.9 as wing vorticity, and ${w_s}^* = -23.5$, -22.7, and -21.8 as secondary vorticity at $h/c = 0.55$, 0.25 and 0.1, respectively. Reductions in peak magnitudes of the vorticity concentrations, ${w_{st}}^*$, ${w_w}^*$ and ${w_s}^*$ of the coiled-up vortices under the GE are also observed at $\alpha = 25°$. Reduction in the peak magnitudes of ${w_{st}}^*$, ${w_w}^*$ and ${w_s}^*$ may be attributed to the insufficient area for the flow to develop further between the wing surface and the ground surface. Furthermore, the magnitude of coiled-up vorticity, w^* concentration at the core region is substantially low. The

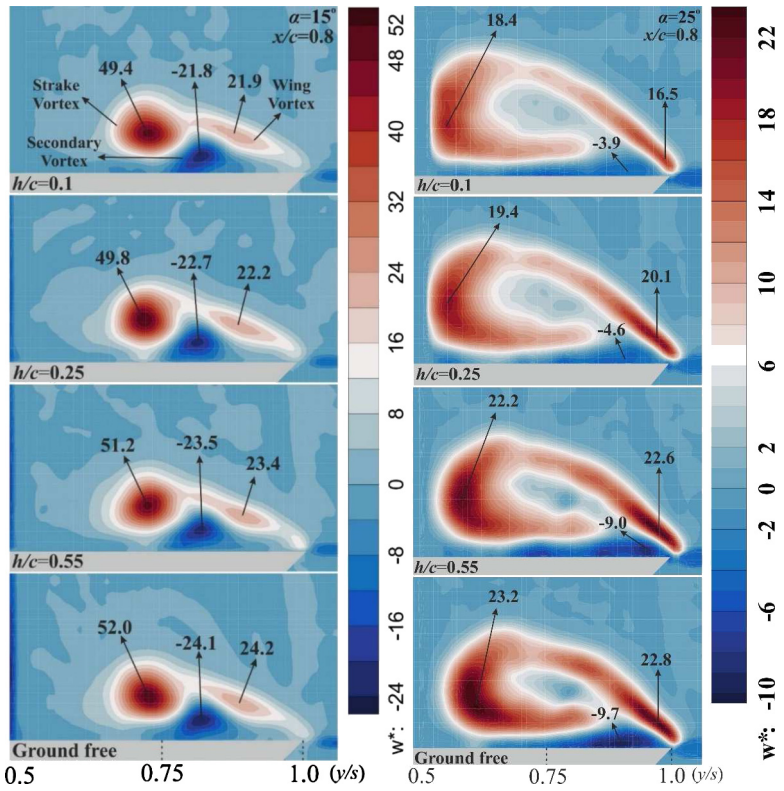

Fig. 9. The alteration of the time-averaged normalized vorticity, w^* concentrations at $\alpha = 15°$ and 25° under the GE with the variations of h/c. (For interpretation of the colors in the figure(s), the reader is referred to the web version of this article.)

reduction in the peak magnitudes can be related to the GE, which causes the coiled-up vortex to induce an earlier stage of VB because of growth in the gradient of the adverse pressure on the bottom of the double delta wing through the chordwise direction. Moreover, the intensity of w^* over the wing decreases with the enhancement in the angle of attack from $\alpha = 15°$ to 25°.

The GE on the flow structure presented in terms of the patterns of the instantaneous streamline, ψ for the GFC and $h/c = 0.1$ at $\alpha = 15°$ are demonstrated in Fig. 10. The three different frames of the instantaneous patterns of the streamlines, ψ are taken to show the instantaneous flow behavior under the GE at different time intervals. It is observed from the instantaneous streamline, ψ patterns that the size of the strake vortex or focus, F_{st} is enlarged when the position of the delta wing lowers from the region of GFC to the level $h/c = 0.1$ where the ground effect is severe. Also, the descending movement of the focus, F_{st} is defined by the instantaneous streamline, ψ patterns simulating the strake vortex, F_{st} occurs with decreasing the ground distance h/c, which is consistent with the patterns of the time-averaged streamline, $< \psi >$. The focus of the secondary vortex, F_s is detected at $h/c = 0.1$ because of the unsteadiness and the growing interaction between the vortical flow and the surface of the double delta wing. The focus of the wing vortex, F_w, moves away from the wing surface, and the height of the focus, F_w increases as the double delta wing gets closer to the ground. Also, the wing vortex moves inboard and interacts more with the strake vortex.

The three different frames of the instantaneous vorticity, ${w_{st}}^*$, ${w_w}^*$ and ${w_s}^*$ concentrations in parallel with patterns of instantaneous streamlines, ψ were taken in the flow region without ground effect, GFC and the flow region under a severe ground effect, GE, for example at $h/c = 0.1$ for $\alpha = 15°$ and $x/c = 0.8$, as shown in Fig. 11. It has been displayed that the unity of the strake, wing, and secondary vorticities, ${w_{st}}^*$, ${w_w}^*$ and ${w_s}^*$ worsens when the wing position is changed from the GFC to a level of $h/c = 0.1$. It is observed that the instantaneous strake vorticity concentration, ${w_{st}}^*$ expands in size resulting in covering the larger region throughout the spanwise direction of the delta wing at $h/c = 0.1$ in comparison with the GFC. Besides, it is indicated that the intensity of the vorticity concentrations, ${w_{st}}^*$, ${w_w}^*$ and ${w_s}^*$ presenting the strake, wing, and secondary vortices become weak with the augmentation of the ground proximity when the double delta wing moves from the free-stream region close to the ground surface, $h/c = 0.1$, because the GE induces the VB at an earlier stage.

As the wing enters the flow region where the ground begins to influence the flow turbulence, the kinetic energy as a function of h/c at $\alpha = 15°$ and 25° was calculated with equation (3).

$$TKE = \frac{1}{2}\left(\frac{\overline{u'^2} + \overline{v'^2}}{U_\infty^2}\right) \tag{3}$$

The obtained results of *TKE* are given in Fig. 12. The conversion of flow energy to heat because of work done by viscous stresses can be validated by the change in the dispersion of the turbulent kinetic energy, which is associated with the degree of turbulence generation in shear flows stated by Canpolat et al. [46]. The variation of large VB fields caused by the gradient of the adverse pressure through the chordwise direction on the pressure surface of the double delta wing is dependent on the ground proximity. The widening flow separation is associated with the flow interference induced by the reduction of the area between the wing surface and the ground surface, which is also stated by Qu et al. [22]. The magnitude of the TKE gets higher with increasing proximity to the ground because of this flow phenomenon explained above. Also, the peak magnitude field of the TKE enlarges throughout the spanwise direction over the wing with an increase of the GE. In summary, the magnitude and the are of TKE distributions along the surface of the wing with decreasing the ground distance, $h/c = 0.1$, is higher in comparison with the GFC. For example, while the peak

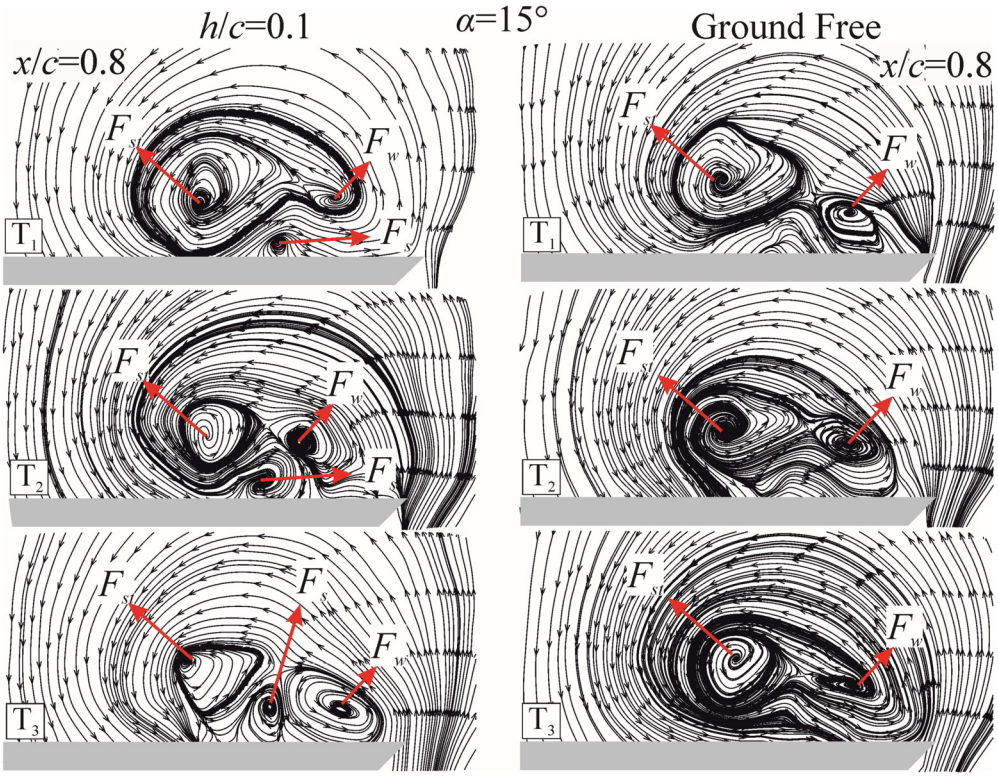

Fig. 10. The instantaneous streamline patterns at $\alpha = 15°$ for the $h/c = 0.1$ case and GFC.

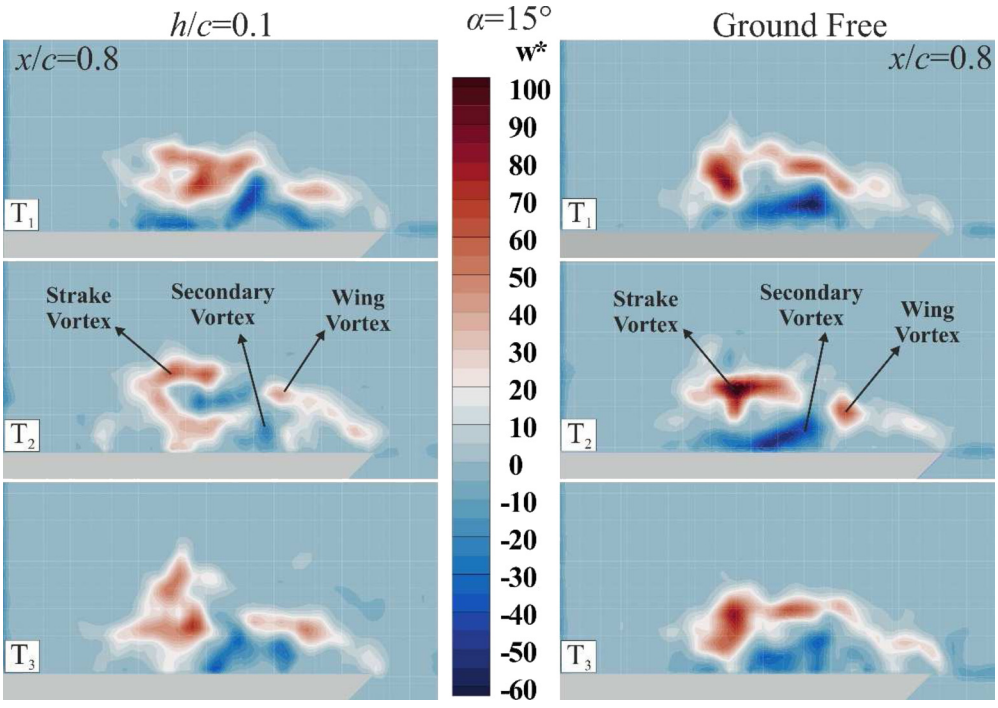

Fig. 11. The instantaneous vorticity concentrations, $w_{st}{}^*$, $w_w{}^*$ and $w_s{}^*$ at $\alpha = 15°$ for $h/c = 0.1$ and GFC.

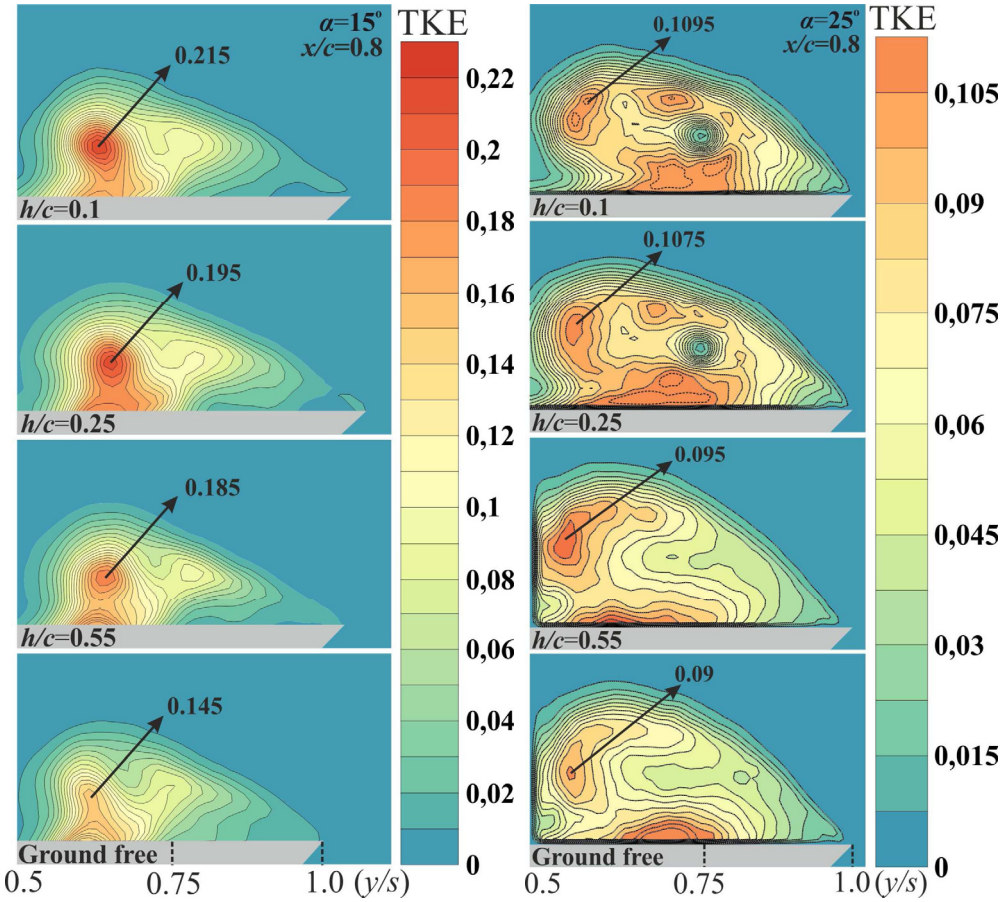

Fig. 12. The alteration of the time-averaged TKE at $\alpha = 15°$ and 25° under the GE with the variations of h/c.

value of TKE at the GFC is found to be 0.145 and 0.09 at $\alpha = 15°$ and 25°, values of TKE at $h/c = 0.1$ due to the severe ground effect increase to levels of 0.215 and 0.1095 at $\alpha = 15°$ and 25°, respectively. Also, the peak value of TKE is found to be higher at $\alpha = 15°$ compared to $\alpha = 25°$.

The GE on the density of the power spectrum (DPS) of the vertical component of the flow velocity, w, in a cross-flow plane at $\alpha = 25°$ is shown in Fig. 13. The Strouhal number, St, is the dimensionless number regarding pulsating flow in the natural environment and is presented as follows:

$$St = \frac{fc}{U_\infty} \tag{4}$$

where c is the chord length of the double delta wing, f is the frequency of vortex shedding at VB, and U_∞ is the free-stream velocity. Since the free-stream velocity, U_∞ and the chord length, c of the double delta wing are constant throughout the experiments, the Strouhal number, St, only varies with the frequency of vortex shedding at the VB. So, the change in the Strouhal number, St can be interpreted by examining variations in the frequency of these vortex shedding at the VB. The dominant peak frequencies were taken in five points (1 to 5). Some criteria are regarded while selecting the locations for PSD analysis. In Figs. 13 and 14, the points in which located in a close region of the surface of the wing, 2 and 3 and the wing's leading edge, 4 are selected for PSD analysis. Furthermore, the points which are located in the middle region of vorticity concentration, for example, point 1 and in the region where high w_{rms} values occur, for example, point 5 are selected for PSD analysis. In the regions where all these selected points are located, significant changes take place in the vortical flow structures over the wing. In Fig. 13, it was seen that the peak frequencies, f of leading-edge vortex breakdown and related Strouhal number, St gradually decrease when the double delta wing approaches extremely close from the unbounded flow region (GFC) to the ground region ($h/c = 0.10$). For instance, the frequency, f of vortex shedding over the double delta wing under the GFC was found as 2.503, 3.944, 3.982, 4.781, and 6.895 Hz, however, f over the double delta wing at $h/c = 0.10$ was detected as 1.207, 3.083, 1.798, 0.823, and 4.316 Hz from points 1 to 5, respectively. Correspondingly, in Fig. 14, it is also seen that the dominant peak frequency, f decreases when the double delta wing moves from the GFC of the flow field to the flow region under the GE. For example, peak frequencies, f over the wing surface in the flow region of the GFC are 1.54, 2.482, 5.603, 3.371, and 2.939 Hz from points 1 to 5, respectively. Likewise, peak frequencies, f under a severe GE at $h/c = 0.10$ are 1.011, 1.093, 1.462, 0.849, and 1.155 Hz from points 1 to 5, respectively. As can be summarized from the results, the value of St decreases by the GE. In other words, the frequency of the vortex shedding at the VB, f decreases. The reduction in St under the GE can be associated with the slowing down of the formation of vortical flow because of intensive interactions between the vortical flow and the delta wing surface. The intensive interaction, the augmentation of flow complexity, and the underdevelopment of vortices over the wing under the GE were reported by Ozden et al. [47]. In the study of Prasad and Damodaran [41], it was expressed that the GE causes a drop in St, which means a decrease in the vortex shedding frequency, f due to a slower vorticity formation through the trailing edge of the NACA-0012 wing.

A comparison of the lift coefficients, C_L of double delta wings with $\Lambda = 70°/40°$ determined in the free-stream within the angles of attack range $5° \leq \alpha \leq 40°$ with previous results reported

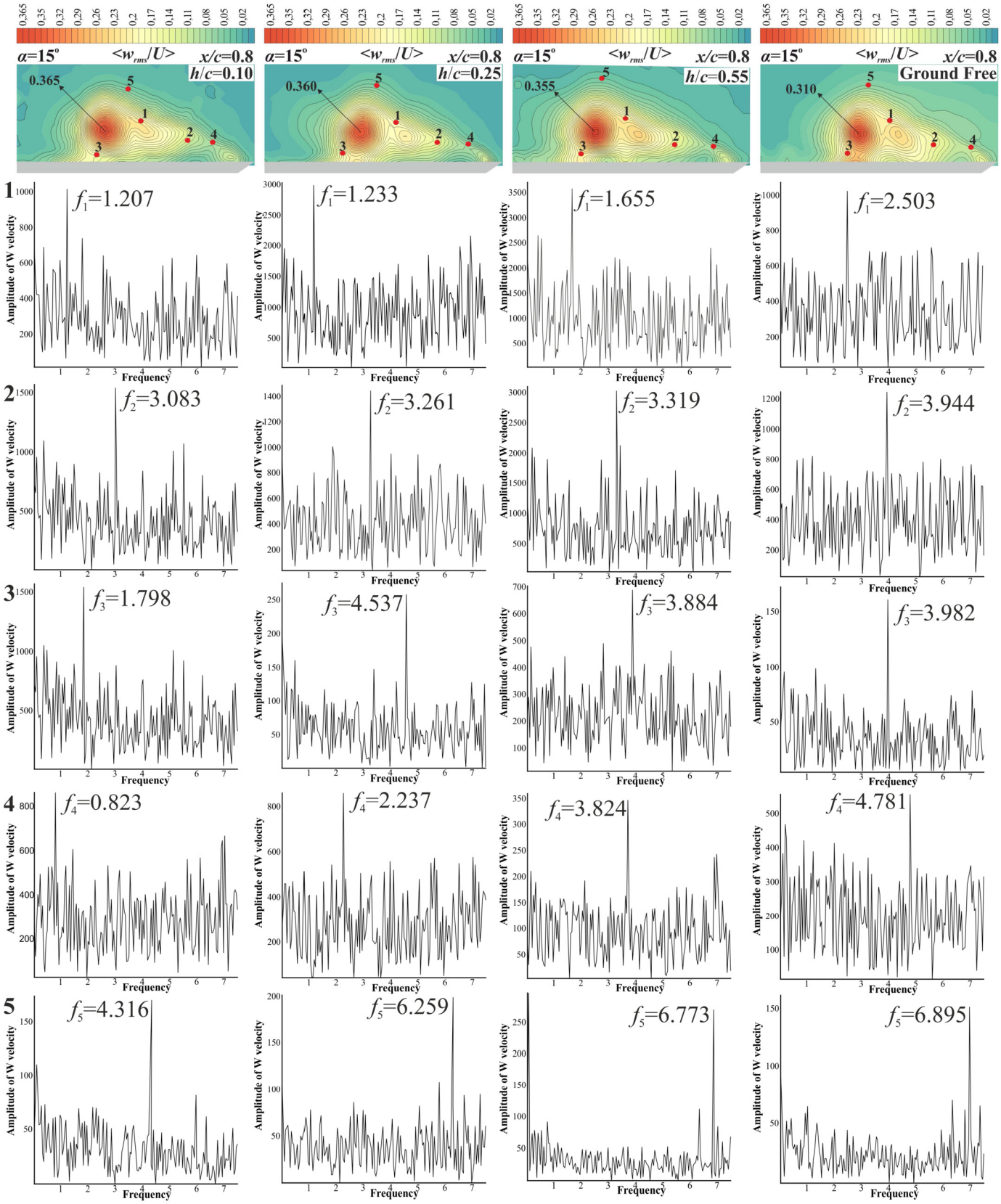

Fig. 13. The alteration of the density of the power spectrum (DPS) of the velocity component in the vertical direction, w at $\alpha = 15°$ under the GE with the variations of h/c.

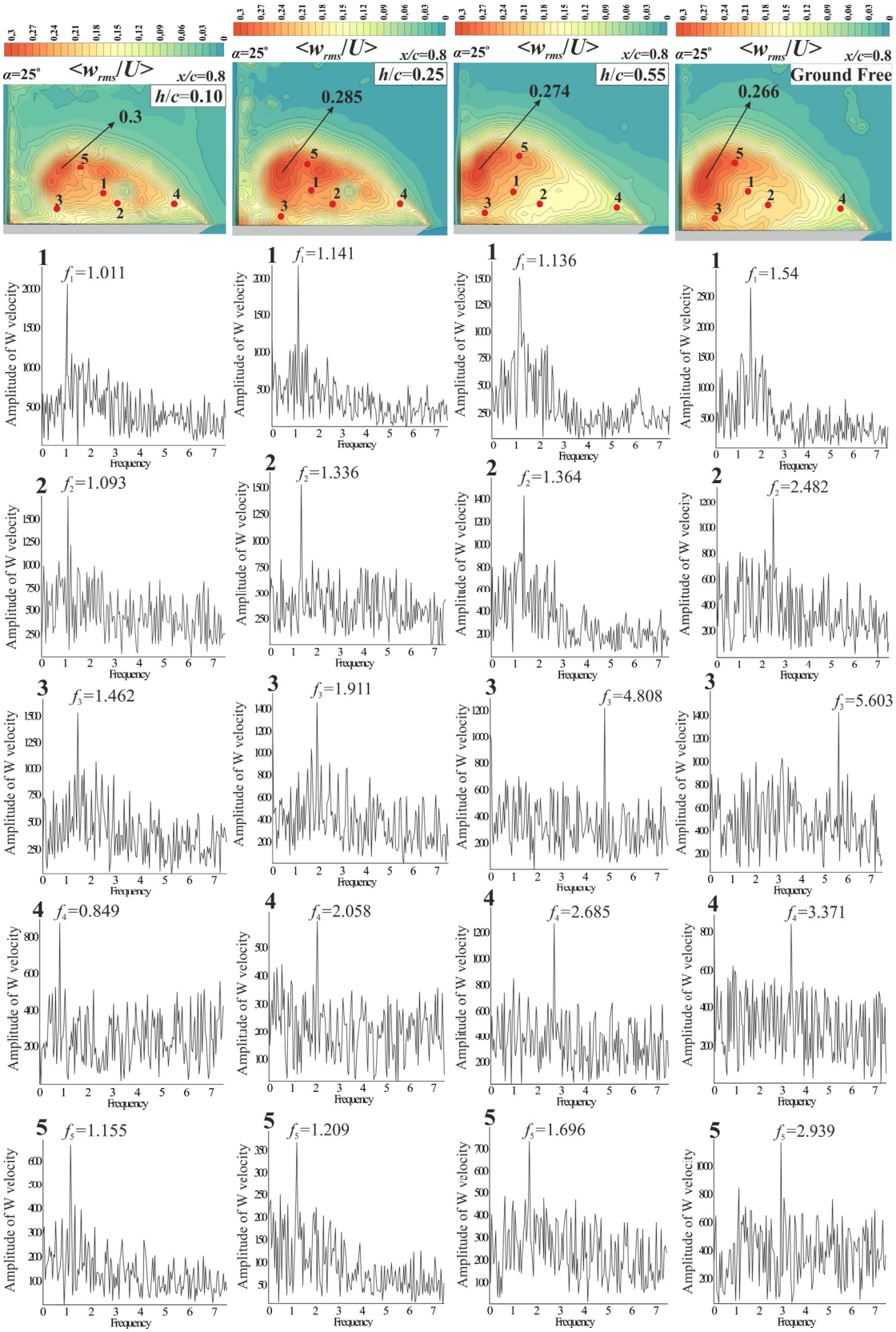

Fig. 14. The alteration of the density of the power spectrum (DPS) of the velocity component in the vertical direction, w at $\alpha = 25°$ under the GE with the variations of h/c.

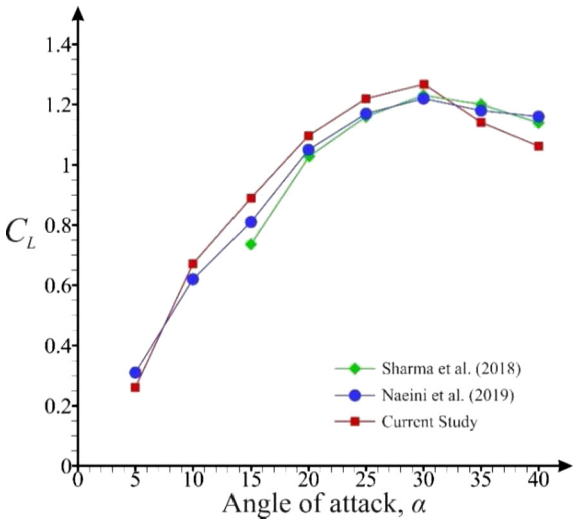

Fig. 15. Comparisons of lift coefficients, C_L of double delta wing measured in free-stream with similar studies reported by Sharma et al. [48] and Naeini et al. [49].

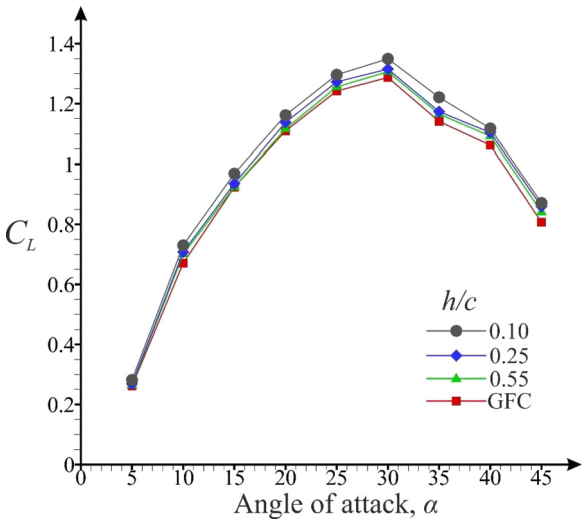

Fig. 16. The alteration of the lift coefficients, C_L of the double delta wing within the range of angles of attack $5° \leq \alpha \leq 45°$ under the GE with the variations of h/c.

by Sharma et al. [48] for sweep angles, $\Lambda = 70°/40°$ and Naeini et al. [49] for sweep angles, $\Lambda = 65°/35°$ are demonstrated in Fig. 15. The lift coefficient, C_L determined experimentaly by Sharma et al. [48] and Naeini et al. [49] were conducted at $Re = 1.89 \times 10^5$ and 2×10^6, respectively. It can be said that the result of the current study is in good agreement with the published studies shown in Fig. 15. It was also observed that the effects of parameters such as experimental uncertainties, geometrical attachments, the thickness/chord ratio, and the bevel angle of the delta wing did not have great effects on the results presented in Fig. 15. For example, in the study of Sharma et al. [48], a rectangular part attached to the trailing edge of the double delta wing having sweep angles $\Lambda = 70°/40°$. Also, the double delta wing with sweep angles $\Lambda = 65°/35°$ tested by Naeini et al. [49] has a bevel angle of 24° at leading edges.

In Figs. 16–18, influences of ground on the aerodynamic properties of the double delta wing having $\Lambda = 70°/40°$ sweep angles are examined under the variations of h/c within the range of angles of attack $5° \leq \alpha \leq 45°$. The variations of lift coefficients, C_L, with altering α under the GE are demonstrated in Fig. 16. The lift coefficient, C_L measured in the flow region with ground effect is slightly larger than the lift coefficient, C_L measured in the region without ground effect on the flow for all examined angles of attack, α. While the double delta wing approaches the stall field at $\alpha = 30°$, C_L gradually grows up when the ground distance, h/c decreases from the flow region of GFC to the $h/c = 0.10$ case where GE on the flow is severe. For example, the percentage of increase in the lift coefficient, ΔC_L between the GFC and the $h/c = 0.1$ case is detected as $\Delta C_L = 4.8\%$, 5.3%, 6.8% when angles of attack, α are adjusted as 15°, 20°, and 30°, respectively. When the double delta wing descends from the GFC flow region into the GE flow region, the values of C_L decrease less in the post-stall flow in comparison with the GFC. For example, percentages of reduction in C_L are 5.3% and 7.9%, at $h/c = 0.1$ for $\alpha = 40°$, and 45°, which are less compared to the GFC. The increase in C_L induced by the GE is considered to be associated with an increase in the ram pressure with increasing proximity to the ground. In addition, the dynamic air cushion formed as a result of the increase in pressure at the base of the wing due to air stagnation in the area between the wing surface and the ground surface strengthens the GE and hence positively affects the aerodynamic properties. The effect of the dynamic air cushion is impaired by reducing the proximity to the ground because of the diminishing ram pressure.

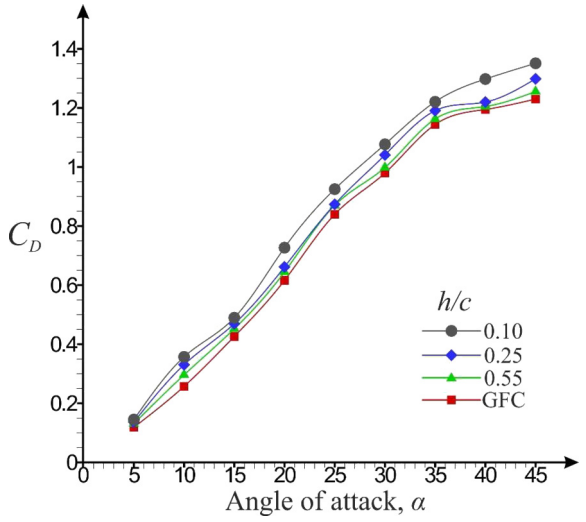

Fig. 17. The alteration of the drag coefficients, C_D of the double delta wing within the range of angles of attack $5° \leq \alpha \leq 45°$ under the GE with the variations of h/c.

In Fig. 17, it is pointed out that strengthening the GE induces a consistently higher drag coefficient, C_D as an independent of α for all ground distance cases. When the higher ground proximity is applied, a higher C_D takes place. The C_D at the extreme ground case, $h/c = 0.10$, is continually greater in comparison with the GFC. For example, the percent increase in the drag coefficient, ΔC_D between the GFC and the $h/c = 0.1$ case are $\Delta C_D = 14.9\%$ and 18% when angles of attack are adjusted as $\alpha = 15°$ and 20°, respectively.

According to Fig. 18, the rise of C_L of the delta wing under GE is suppressed by the increase in C_D and this event induces the existence of lower C_L/C_D for the delta wing under GE compared to the case of GFC. For example, the value of C_L/C_D is maximum for GFC, and it attenuates when the delta wing progressively lowers from the free-flight region into the ground effect region, i.e., from $h/c = 0.55$ to $h/c = 0.1$. Furthermore, obtained results demonstrated that the augmentation of C_L/C_D with GFC is significantly higher at lower angles of attack, α because the leading-edge vortex breakdown takes place in the region close to the delta wing apex at higher angles of attack, α. This event attenuates the aerodynamic efficiency of the slender delta wing significantly at higher α's.

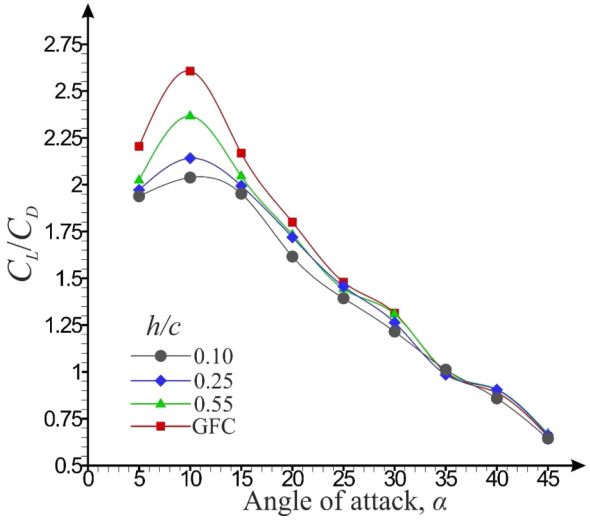

Fig. 18. The alteration of the lift-to-drag ratio, C_L/C_D for the double delta wing within the range of angles of attack $5° < \alpha < 45$ under the GE with the variations of h/c.

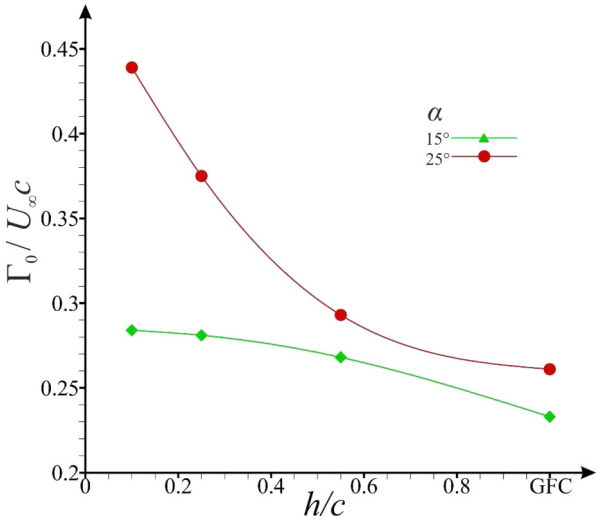

Fig. 19. The alteration of the total circulation under the GE with the variations of h/c at $\alpha = 15°$ and 25°.

The variation of the total circulation under the GE with variations of h/c at $\alpha = 15°$ and 25° is specified in Fig. 19. The total circulation of LEV, Γ_o is computed by the Stokes theorem which is demonstrated in Eq. (5);

$$\Gamma_o = \oint_C \vec{u}.d\vec{x} = \int_A [\nabla \times \vec{u}].\hat{n}dA = \int_A \vec{\omega}.\hat{n}dA \tag{5}$$

in which Γ_o is the value of the LEV total circulation around an enclosed curve, C, $\vec{u}$ is the velocity vector that is randomly oriented, and the projection of $\vec{u}$ in the direction of $d\vec{x}$ can be acquired by getting the scalar product between two vectors. Furthermore, $d\vec{x}$ is the differential line element vector throughout C, $\vec{\omega}$ is the vorticity vector, A is the area surrounded by vorticity contour. The magnitude of Γ_o is nondimensionalized with the product of wing chord length, c and free-stream velocity, U_∞ as $\Gamma_o/U_\infty c$.

The variation of the total circulation, Γ_o is associated with the aerodynamic characteristics of the vortical flow over the wing, and it is normalized by dividing with free-stream velocity, U_∞, and the chord length of the wing, c. As indicated in Fig. 19, the dimensionless total circulation, $\Gamma_o/U_\infty\ c$ on the double delta wing dramatically augments when the angle of attack increases from $\alpha = 15°$ to 25°, which is compatible with the high C_L at a high α. For example, the value of the total circulation increases from 0.285 to 0.44 when α is varied from 15° to 25° at the $h/c = 0.1$ case. An increment in dimensionless total circulation, $\Gamma_o/U_\infty\ c$, under the GE, is also coherent with the augmentation in the C_L. The total circulation, $\Gamma_o\ /\ U_\infty\ c$, progressively enhances when the proximity to the ground increases because of the ram pressure, as pointed out by Gursul and Wang [50]. For example, overall increments in the total circulation, $\Gamma_o/U_\infty\ c$, are 21.3% and 66% when the position of the double delta wing is varied from the GFC field to the GE field at $\alpha = 15°$ and 25°, respectively.

The results of the ground surface impact on the magnitude and the distribution of dimensionless time-averaged velocity vectors, $< V > /U_\infty$ over the delta wing under the variations of h/c at $\alpha = 25°$ are given in Fig. 20. The three examined locations, 1, 2 and 3 were selected according to their importance in terms of flow behaviors on the time-averaged streamline, $< \psi >$ distribution which is shown on the left side of Fig. 20. For instance, the selected lines of 2 and 3, are especially effective locations on the flow structure of the delta wing. The examined line 2 passes through the focal point of the coiled-up vortex center and the examined line 3 is located in the region very close to the wing surface where there is a fluid-structure interaction affecting the aerodynamic performance of the wing considerably. The examined line 1 is arbitrarily chosen to detect the variation of $< V > /U_\infty$ far away from the wing surface and focus point. The $< V > /U_\infty$ is lower at the leading edge of the wing in comparison with the area towards the central axis for all selected locations on the double delta wing. Moreover, it is indicated that the $< V > /U_\infty$ diminishes in Line 3, in comparison with Lines 1 and 2. As shown in Fig. 20, it is observed that the dimensionless value of time-averaged velocity vectors $< V > /U_\infty$ increases in most of the vortical flow regions, especially in the close area to the central axis of the wing such as Lines 1, 2, and 3. The ram pressure caused by the dynamic air cushion between the ground and the bottom of the double delta wing slows down the fluid motion near the leading edge of the wing and induces the flow to move inboard towards the wing's central axis along the spanwise. The $< V > /U_\infty$ decreases because the GE causes an earlier VB when the double delta wing moves from the flow region of GFC to the flow region under the GE. Therefore, the velocity of the flow field increases towards the central axis of the wing because of the ram pressure.

4. Conclusion

Experimental investigations were conducted to see the influences of the ground surface on the formation of the vortical flow over a double delta wing having a sweep angles ratio of $\Lambda = 70°/40°$ with the alteration of the ground distance, h/c. Dye observations and instantaneous flow measurements using the PIV technique in the water channel and force measurements in the wind tunnel were carried out. The chordwise location over the cross-flow plane was taken as $x/c = 0.8$ for all experiments. Since high angles of attack, α cause the double delta wing to develop the stalled flow, the possibility of the identification of the strake, wing, and secondary vortices become challenging, and it is also revealed that the vortices start to move in a large coherent vortex form, which is named as "coiled-up vortex" when the angle of attack alters from $\alpha = 15°$ to 25°. The occurrence of the VB at an earlier stage over the double delta wing with the alteration of the ground distance, h/c under the GE, was noticed in comparison with the GFC at $\alpha = 25°$. The GE induces the breakdown of the coiled-up vortex to form at an earlier stage due to the increase in the gradient of the adverse pressure on the bottom of the double delta wing through the chordwise direction. The vortex

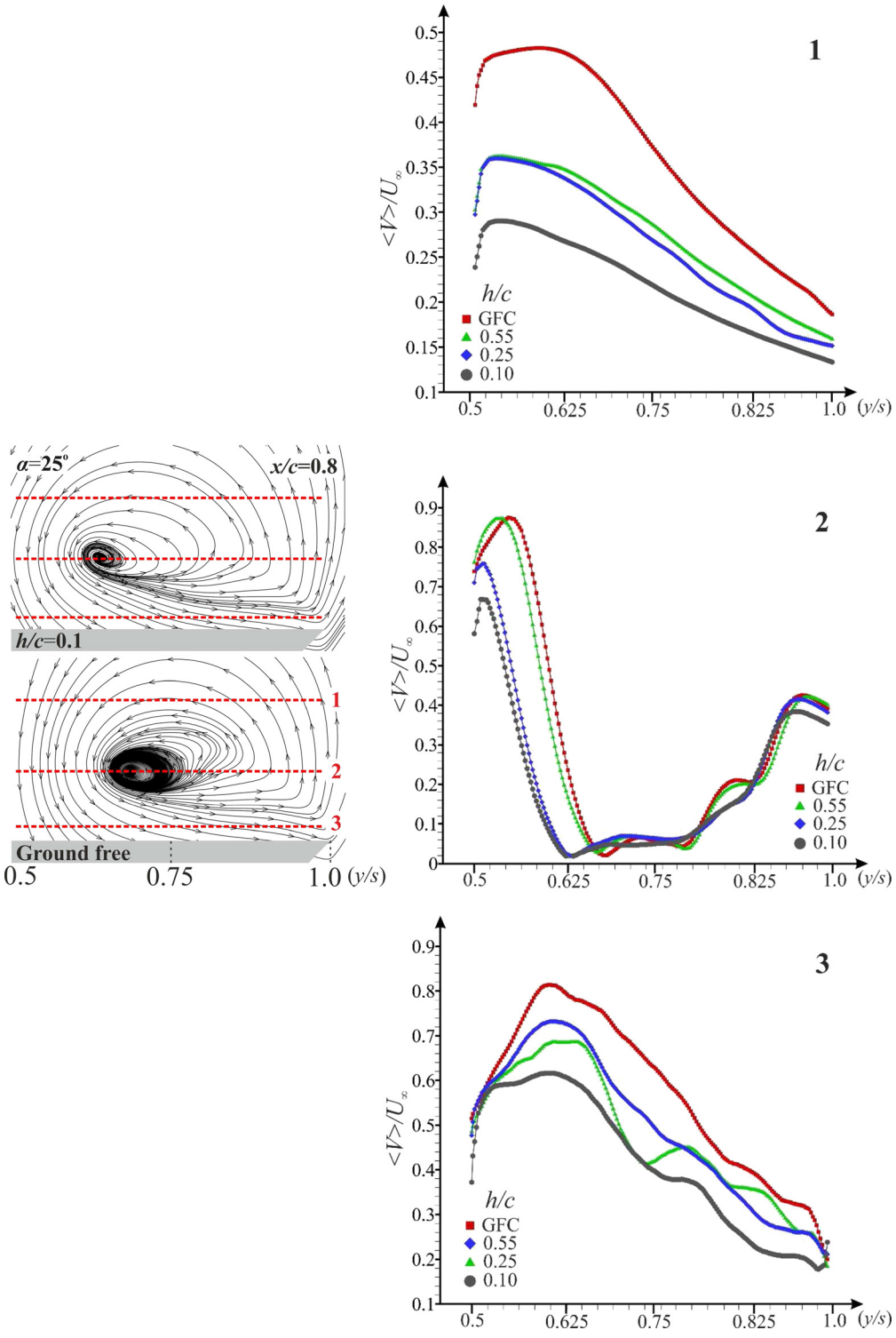

Fig. 20. The alteration of the normalized magnitude of time-averaged velocity vectors, $< V > /U_\infty$ on the cross-flow plane for three selected locations, 1, 2 and 3 at $\alpha = 25°$ with the variation of h/c.

oscillation increases with the irregularities in the flow as the double delta wing descends to the flow field affected by the presence of the ground surface. The dynamic air cushion causes the wing vortex to move away from the wing surface, although the interaction rate between the wing surface and the ground increases. Also, the inboard movement of the coiled-up vortex from the leading-edge side to the wing central axis along the spanwise direction over the double delta wing occurs when the delta wing position is altered from the region of GFC to the case of $h/c = 0.1$. The magnitudes of strake, ${w_{st}}^*$ wing, ${w_w}^*$ and secondary vorticities, ${w_s}^*$ progressively diminish as the double delta wing moves from ground free flow region towards the flow region where ground effect exists at both angles of attack $\alpha = 15°$ and 25°. Reduction in peak magnitudes of ${w_{st}}^*$, ${w_w}^*$ and ${w_s}^*$ may be dependent on the insufficient area for the flow to develop between the wing surface and the ground surface. It is seen that the peak magnitudes of the TKE appear to spread over a wider area throughout the spanwise direction of the double delta wing under the strengthening of the GE as a function of h/c in comparison with the GFC. It was observed from the density of power spectrum (DPS) analysis that when the delta wing approaches the ground surface, the values of the dominant peak frequency, f of vortex shedding at the VB decrease. Since the Strouhal number, St decreases because of the slowing down of the formation of the vortical flow over the double delta wing with increasing the proximity to the ground. The lift coefficient, C_L measured in the flow region with the ground effect is slightly larger than the lift coefficient, C_L measured in the region without the ground effect on the flow for all examined angles of attack, α. The strengthening of the GE induces the drag coefficient, C_D, to increase for all angles of attack, α. Obtained results demonstrated that the augmentation of C_L/C_D together with GFC and GE cases is significantly higher at lower angles of attack, α because the leading-edge vortex breakdown takes place in the region close to the delta wing apex at higher angles of attack, α. This event attenuates the aerodynamic efficiency of the slender delta wing significantly at higher α's. The dimensionless total circulation, $\Gamma_o \mid U_\infty\ c$ on the double delta wing dramatically augments when the angle of attack increases from $\alpha = 15°$ to 25°, which is compatible with a high C_L at high angles of attack, α. The dimensionless total circulation, $\Gamma_o \mid U_\infty\ c$, progressively enhances when the proximity to the ground increases because of the ram pressure. Finally, the normalized magnitude of time-averaged velocity vectors, $< V > /U_\infty$ is lower at the leading edge of the wing in comparison with the area towards the central axis for all selected locations on the double delta wing.

Declaration of competing interest

The authors declare that they have no known competing financial interests or personal relationships that could have appeared to influence the work reported in this paper.

Data availability

Data will be made available on request.

Acknowledgements

The research described in this paper was financially supported by the Scientific Research Project Office of Çukurova University under contract no: FDK-2019-11368. The authors are grateful to the Department of Energy Systems Engineering of Osmaniye Korkut Ata University for allowing the use of PIV and flow visualization systems. Furthermore, the authors would like to thank the Mechanical Engineering Department of Nigde Omer Halisdemir University for allowing the wind tunnel for force measurements. One of the authors has been granted by the TÜBİTAK (The Scientific and Technological Research Council of Turkey) through a Doctoral Researcher Program with project number 2211-C. The author is grateful to The Scientific and Technological Research Council of Turkey for this support.

References

[1] I. Gursul, Review of unsteady vortex flows over slender delta wings, J. Aircr. 42 (2) (2005) 299–319.
[2] I. Gursul, M.R. Allan, K.J. Badcock, Opportunities for the integrated use of measurements and computations for the understanding of delta wing aerodynamics, Aerosp. Sci. Technol. 9 (3) (2005) 181–189.
[3] J.M. Delery, Aspects of vortex breakdown, Prog. Aerosp. Sci. 30 (1) (1994) 1–59.
[4] C.D. Munro, P. Krus, C. Jouannet, Implications of scale effect for the prediction of high angle of attack aerodynamics, Prog. Aerosp. Sci. 41 (3–4) (2005) 301–322.
[5] C. Pevitt, F. Alam, Static computational fluid dynamics simulations around a specialized delta wing, Comput. Fluids 100 (2014) 155–164.
[6] Y.D. Cui, T.T. Lim, H.M. Tsai, Control of vortex breakdown over a delta wing using forebody spanwise slot blowing, AIAA J. 45 (1) (2007) 110–117, https://doi.org/10.2514/1.22575.
[7] F.M. Payne, T. Ng, R.C. Nelson, L.B. Schiff, Visualization and wake surveys of vortical flow over a delta wing, AIAA J. 26 (2) (1988) 137–143.
[8] M.M. Yavuz, M. Elkhoury, D. Rockwell, Near-surface topology and flow structure on a delta wing, AIAA J. 42 (2) (2004) 332–340.
[9] M. Ozgoren, B. Sahin, D. Rockwell, Vortex structure on a delta wing at high angle of attack, AIAA J. 40 (2002) 285–292.
[10] I. Karasu, S. Tumse, M.O. Tasci, B. Sahin, H. Akilli, Near-surface particle image velocimetry measurements over a yawed slender delta wing, Proc. Inst. Mech. Eng., G J. Aerosp. Eng. 235 (16) (2021) 2466–2478.
[11] M. Oguz Tasci, S. Tumse, B. Sahin, Vortical flow characteristics of a slender delta wing in ground effect, Ocean Eng. 261 (2022) 112120.
[12] G. Kocak, M.M. Yavuz, Aerodynamics of non-slender Delta and reverse delta wings: wing thickness, anhedral angle and cropping ratio, Chin. J. Aeronaut. (2022).
[13] G.S. Taylor, I. Gursul, Buffeting flows over a low-sweep delta wing, AIAA J. 42 (9) (2004) 1737–1745.
[14] B. Sahin, S. Yayla, C. Canpolat, H.Ü. Akilli, Flow structure over the yawed non-slender diamond wing, Aerosp. Sci. Technol. 23 (1) (2012) 108–119.
[15] M.O. Tasci, M.C. Pektas, S. Tumse, I. Karasu, B. Sahin, H. Akilli, The impact of the pitching motion on the structure of the vortical flow over a slender delta wing under sideslip angle, J. Vis. 24 (3) (2021) 437–442.
[16] M. Le Sueur, Ground Effect on the Take-Off and Landing of Airplanes, National Advisory Committee for Aeronautics, Washington, DC, 1935.
[17] K. Chawla, W.R. Van Dalsem, K.V. Rao, Simulation of a delta wing with two jets in ground effect, Comput. Syst. Eng. 1 (2–4) (1990) 483–494.
[18] Z. Yang, W. Yang, Y. Li, Analysis of two configurations for a commercial WIG craft based on CFD, in: 27th AIAA Applied Aerodynamics Conference, 2009, p. 4112.
[19] S.C. Luo, Y.S. Chen, Ground effect on flow past a wing with a NACA0015 cross-section, Exp. Therm. Fluid Sci. 40 (2012) 18–28.
[20] Y. Qin, Q. Qu, P. Liu, Y. Tian, Z. Lu, DDES study of the aerodynamic forces and flow physics of a delta wing in static ground effect, Aerosp. Sci. Technol. 43 (2015) 423–436.
[21] Y. Qin, P. Liu, Q. Qu, H. Guo, Numerical study of aerodynamic forces and flow physics of a delta wing in dynamic ground effect, Aerosp. Sci. Technol. 51 (2016) 203–221.
[22] Q. Qu, Z. Lu, H. Guo, P. Liu, R.K. Agarwal, Numerical investigation of the aerodynamics of a delta wing in ground effect, J. Aircr. 52 (1) (2015) 329–340.
[23] Q. Jia, W. Yang, Z. Yang, Numerical study on aerodynamics of banked wing in ground effect, Int. J. Naval Archit. Ocean Eng. 8 (2) (2016) 209–217.
[24] C.M. Velte, M.O. Hansen, V.L. Okulov, Multiple vortex structures in the wake of a rectangular winglet in ground effect, Exp. Therm. Fluid Sci. 72 (2016) 31–39.
[25] L.S. Ko, V. Tremblay-Dionne, T. Lee, Impact of ground proximity on an inverted delta wing, J. Aerosp. Eng. 33 (5) (2020) 04020047.
[26] T. Lee, L.S. Ko, Ground effect on the vortex flow and aerodynamics of a slender delta wing, J. Fluids Eng. 140 (7) (2018).
[27] T. Lee, S.M. He, The trailing vortices are generated by a reverse delta wing with different wing configurations, Aerosp. Sci. Technol. 82 (2018) 378–393.
[28] L. Wang, R.W. Yeung, Investigation of full and partial ground effects on a flapping foil hovering above a finite-sized platform, Phys. Fluids 28 (7) (2016) 071902.
[29] R. Bleischwitz, R. De Kat, B. Ganapathisubramani, Near-wake characteristics of rigid and membrane wings in ground effect, J. Fluids Struct. 80 (2018) 199–216.
[30] L. Bricteux, M. Duponcheel, I. De Visscher, G. Winckelmans, LES investigation of the transport and decay of various-strengths wake vortices in ground effect and subjected to a turbulent crosswind, Phys. Fluids 28 (6) (2016) 065105.

[31] S. Tumse, M.O. Tasci, I. Karasu, B. Sahin, Effect of ground on flow characteristics and aerodynamic performance of a non-slender delta wing, Aerosp. Sci. Technol. 110 (2021) 106475.
[32] B. Yin, G. Yang, P. Prapamonthon, Finite obstacle effect on the aerodynamic performance of a hovering wing, Phys. Fluids 31 (10) (2019) 101902.
[33] A. Pelletier, R. Nelson, Dynamic behavior of an 80-deg/65-deg double-delta wing in roll, in: Proc., 23rd Atmospheric Flight, 1998.
[34] M.D. Manshadi, M. Eilbeigi, M.K. Sobhani, M.B. Zadeh, M.A. Vaziry, Experimental study of flow field distribution over a generic cranked double delta wing, Chin. J. Aeronaut. 29 (5) (2016) 1196–1204.
[35] I. Karasu, T. Durhasan, Flow characteristics over double Delta wings at low Reynolds numbers, J. Aerosp. Eng. 33 (4) (2020) 04020038.
[36] T. Durhasan, İ. Karasu, Dye visualization over double delta wing with various kink angles, J. Vis. 22 (4) (2019) 669–681.
[37] J. Liu, H. Sun, Z. Liu, Z. Xiao, Numerical investigation of unsteady vortex breakdown past 80/65 double-delta wing, Chin. J. Aeronaut. 27 (3) (2014) 521–530.
[38] X. Zhang, Z. Wang, I. Gursul, Interaction of multiple vortices over a double delta wing, Aerosp. Sci. Technol. 48 (2016) 291–307.
[39] X. Zhang, Z. Wang, I. Gursul, Control of multiple vortices over a double delta wing, in: 47th AIAA Fluid Dynamics Conference, 2017, p. 4122.
[40] S. Tumse, I. Karasu, B. Sahin, Experimental investigation of ground effect on the vortical flow structure of a 40° swept Delta Wing, J. Aerosp. Eng. 35 (4) (2022).
[41] R. Prasad, M. Damodaran, Computational modelling of steady and unsteady low speed wing in ground effect aerodynamics, in: 51st AIAA Aerospace Sciences Meeting Including the New Horizons Forum and Aerospace Exposition, 2013, p. 497.
[42] M.R. Ahmed, S.D. Sharma, An investigation on the aerodynamics of a symmetrical airfoil in ground effect, Exp. Therm. Fluid Sci. 29 (6) (2005) 633–647.
[43] Meinhart, Soloff, Cleanvec Software, Turbulence Laboratory, University of Illinois at Urbana-Champaign, 1999.
[44] N.A. Ozturk, A. Akkoca, B. Sahin, Flow details of a circular cylinder mounted on a flat plate, J. Hydraul. Res. 46 (3) (2008) 344–355.
[45] R.J. Moffat, Describing the uncertainties in experimental results, Exp. Therm. Fluid Sci. 1 (1) (1988) 3–17.
[46] C. Canpolat, S. Yayla, B. Sahin, H. Akilli, Observation of the vortical flow over a yawed delta wing, J. Aerosp. Eng. 25 (4) (2012) 613–626.
[47] K.S. Ozden, İ. Karasu, M.S. Genç, Experimental investigation of the ground effect on a wing without/with trailing edge flap, Fluid Dyn. Res. 52 (4) (2020) 045504.
[48] B. Sharma, R.N. Barman, T. Murugan, Experimental and Numerical Investigation of Flow over 70/40 Double Delta Wing at Low Reynolds Numbers, 2018.
[49] H.K. Naeini, M. Nili-Ahmadabadi, K.C. Kim, An experimental study on the effect of a novel nature-inspired 3D-serrated leading edge on the aerodynamic performance of a double delta wing in the transitional flow regime, J. Mech. Sci. Technol. 33 (12) (2019) 5913–5921.
[50] I. Gursul, Z. Wang, Flow control of tip/edge vortices, AIAA J. 56 (5) (2018) 1731–1749.
[51] C. Canpolat, S. Yayla, B. Sahin, H. Akilli, Dye visualization of the flow structure over a yawed nonslender delta wing, J. Aircr. 46 (5) (2009) 1818–1822.